applied sciences

MDPI

Article

Mitigating the Impact of Asymmetric Deformation on Advanced Metrology for Photolithography

Wenhe Yang [1,2,3,†], Shuxin Yao [4,†], Jing Cao [2,3] and Nan Lin [1,2,3,*]

[1] School of Microelectronics, Shanghai University, Shanghai 200072, China; sdwdzywh@shu.edu.cn
[2] State Key Laboratory of High Field Laser Physics, Shanghai Institute of Optics and Fine Mechanics, Chinese Academy of Sciences, Shanghai 201800, China; caojing0606@siom.ac.cn
[3] Key Laboratory of Ultra-Intense laser Science and Technology (CAS), Shanghai 201800, China
[4] School of Microelectronics, Fudan University, Shanghai 200433, China; 18112020054@fudan.edu.cn
* Correspondence: nanlin@siom.ac.cn
† These authors contributed equally to this work.

Abstract: Controlling overlay in lithography is crucial for improving the yield of integrated circuit manufacturing. The process disturbances can cause undesirable morphology changes of overlay targets (such as asymmetric grating), which can significantly impact the accuracy of overlay metrology. It is essential to decouple the overlay target asymmetry from the wafer deformation, ensuring that the overlay metrology is free from the influence of process-induced asymmetry (e.g., grating asymmetry and grating imbalance). Herein, we use an asymmetric grating as a model and show that using high-diffraction-order light can mitigate the impact of asymmetric grating through the rigorous coupled-wave analysis (RCWA) method. In addition, we demonstrate the diffraction efficiency as a function of the diffraction order, wavelength, and pitch, which has guiding significance for improving the measurement accuracy of diffraction-based overlay (DBO) metrology.

Keywords: edge placement error; diffraction-based overlay; extreme ultraviolet (EUV) lithography; measurement; alignment

Citation: Yang, W.; Yao, S.; Cao, J.; Lin, N. Mitigating the Impact of Asymmetric Deformation on Advanced Metrology for Photolithography. *Appl. Sci.* **2024**, *14*, 4440. https://doi.org/10.3390/app14114440

Academic Editor: Arkadiusz Gola

Received: 8 March 2024
Revised: 25 April 2024
Accepted: 28 April 2024
Published: 23 May 2024

1. Introduction

With the evolution of Moore's Law, the feature of the semiconductor device continues to shrink [1]. It is essential to reduce the edge placement error (EPE) to maintain the performance and high yield of a device [2,3]. EPE serves as a metric for quantifying the fidelity of lithography technology and the EPE budget decreases with the iteration of the logic node [4–6]. EPE is a combination of critical dimension (CD) errors and overlay errors [5–7]. With the increase of the process complexity, more space has been reserved for components such as optical proximity error and photon and resist stochastics [5]. In particular, for the most advanced node (e.g., EUV lithography), typically, EPE is dominated by stochastics (>50%) [3,8]. In contrast, the overlay consumption decreases from 34% (for 9~13 nm logic nodes) to 21% (for 5~7 nm logic nodes) of the EPE budget [2,6]. Therefore, the improvement of overlay performance is an efficient approach to reducing EPE.

Overlay refers to the alignment deviation of the patterns between different layers, which has a significant impact on the quality of integrated circuits (e.g., short circuits and open circuits) [9]. For single exposure, the overlay budget typically amounts to a quarter of the half pitch, while for double patterning, the overlay budget is one-sixth of the half pitch [5]. Currently, the accuracy required for measuring overlay needs to meet the demand of the sub-nanometer level for chip manufacturing [10]. The control of overlay mainly involves three steps: alignment, after-development inspection (ADI), and after-etch inspection (AEI) [11]. The sampling requirement for ADI is relatively high (~4 wafers per lot, with 800 measurement points per wafer); the sampling requirement for AEI is slightly low (~2 wafers measured within a few days, with 10^4 measurement points on

each wafer) [12]. Overlay metrology can be used to detect unwanted positional shifts and process variation between layers. It is an important part of the process control in advanced semiconductor manufacturing [13].

To ensure high yield, inline metrology is crucial in high-volume manufacturing (HVM) [14]. HVM overlay advanced process control is mainly based on optical metrology at the ADI step, such as imaging-based overlay (IBO) and diffraction-based overlay (DBO) [15]. In addition, a high-voltage scanning electron microscope (SEM) was used at the ADI and AEI steps, as well as AEI in die overlay measurement [15,16]. However, SEM has the problem of low throughput and destructive testing. IBO has played a crucial role in overlay metrology, but it faces numerous challenges [17]. DBO is receiving the most attention because of its superior measurement accuracy [18,19]. Various methods have been proposed for DBO, such as multi-wavelength measurement [20] and DBO target design (e.g., μDBO and cDBO) [21].

DBO is traditionally performed by measuring the interference signal of the ±1st diffraction order light that is diffracted by the top and bottom structures to obtain the value of overlay [22]. The accuracy of the overlay could be influenced by the asymmetry of the overlay target [13,23]. It is essential to decouple the overlay target asymmetry from the wafer deformation, ensuring that overlay metrology is free from the influence of process-induced asymmetry (e.g., grating asymmetry and grating imbalance) [6]. Optimizing overlay target design is an accepted way to reduce the impact of the process (e.g., etching, deposition, and chemical mechanical polishing) [13,24]. This method is designed before exposure and process-induced asymmetric deformation of the overlay target occurs often. Therefore, it is significant in improving the measurement accuracy for the asymmetric grating that is produced after exposure.

Herein, we use an asymmetric grating as a model and demonstrate that using high-diffraction-order light can mitigate the measurement impact of asymmetric grating. In addition, we demonstrate the diffraction efficiency as a function of the diffraction order, wavelength, and pitch. Additionally, we explore the overlay target materials.

2. Model Creation

For ADI, it is assumed that the morphology of the top grating is symmetrical (as shown in Figure 1a), which consists of a uniform photoresist or anti-reflection coating, due to undergoing various planar process steps such as spin-coating and resist coating [24,25]. In contrast, the asymmetric deformation of bottom grating frequently occurs [13]. The tilt angle is represented by the symbol ϕ, the grating groove depth is represented by the symbol h, the symbol p refers to the pitch, and the duty cycle is defined as a/p. The h value was chosen to be 80 nm [26]. The duty cycle was 0.5. The pitch was chosen as 6000 nm, 3000 nm, 1600 nm, 1200 nm, 1000 nm, 900 nm, 800 nm, 700 nm, and 600 nm, respectively. The wavelength ranged from 160 to 200 nm or 360 to 600 nm, depending on the pitch. The light was linearly polarized and the grating axis was aligned parallel to the laser polarization direction.

The diffraction values of the light intensity of positive ($I_{+1\text{top}}$) and negative ($I_{-1\text{top}}$) diffraction order, generated by the top grating with symmetric morphology, were equal. The use of multi-wavelength measurements to measure overlay in advanced DBO can ensure that the interference between the top light and the bottom light (i.e., I_{top} and I_{bottom}) of the composite light intensity source is enhanced at a certain wavelength. The error signal only comes from the impact of the asymmetric bottom grating. Thus, we used an asymmetric grating as a model to investigate how to mitigate the impact of asymmetric deformation of the bottom grating (see Figure 1b) in the overlay metrology. The overlay error was set to 0. At normal incidence, the asymmetric grating shows asymmetric diffraction into the positive and negative diffraction orders. An error signal, caused by the asymmetric grating, is expressed by the difference in the diffraction efficiency of positive and negative diffracted light (±1st through ±4th diffraction order). To compare, we also provided the error signal for the symmetric grating. Rigorous coupled-wave analysis (RCWA) is one

of the widely used methods for the modeling of diffraction gratings [27]. The diffraction efficiency was analyzed using RCWA. In this study, GSolver (GSolver V5.2) was employed for the simulation [28].

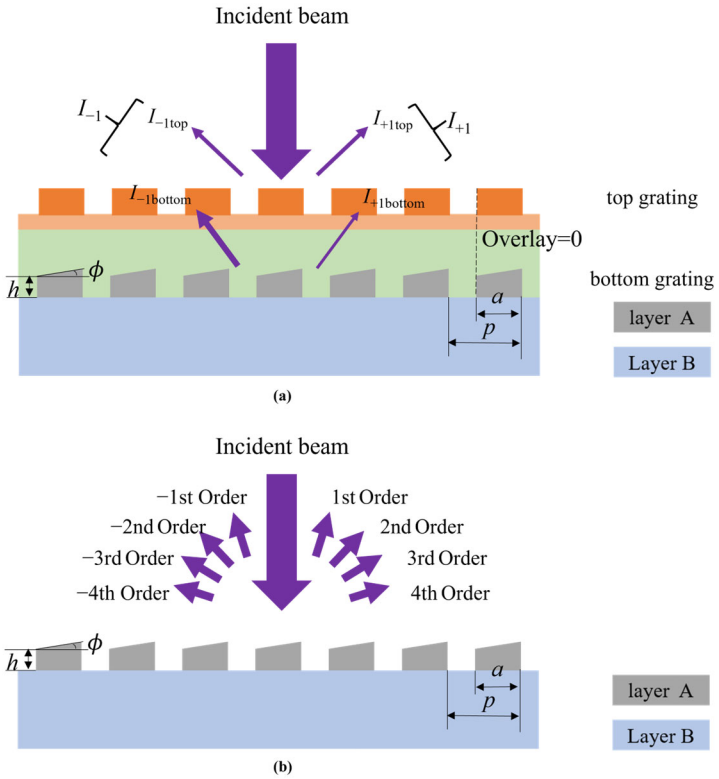

Figure 1. Schematic diagram of the cross section of (**a**) an overlay target and (**b**) diffraction from an asymmetric bottom grating. ϕ: tilt angle, h: grating groove depth, p: pitch, and a/p: duty cycle, normal incidence.

One of the trends in overlay metrology is to use new materials for fabricating overlay targets, aiming to increase the signal-to-noise ratio (S/N) and sensitivity of overlay measurement [15]. In this simulation, aluminum (Al) was applied for Layer A, and silicon nitride (Si_3N_4) or silicon dioxide (SiO_2) was applied for Layer B (see Figure 1), respectively. The index of refractive (n) and extinction coefficient (k) versus wavelength of Si_3N_4 and SiO_2 were shown in Figure 2.

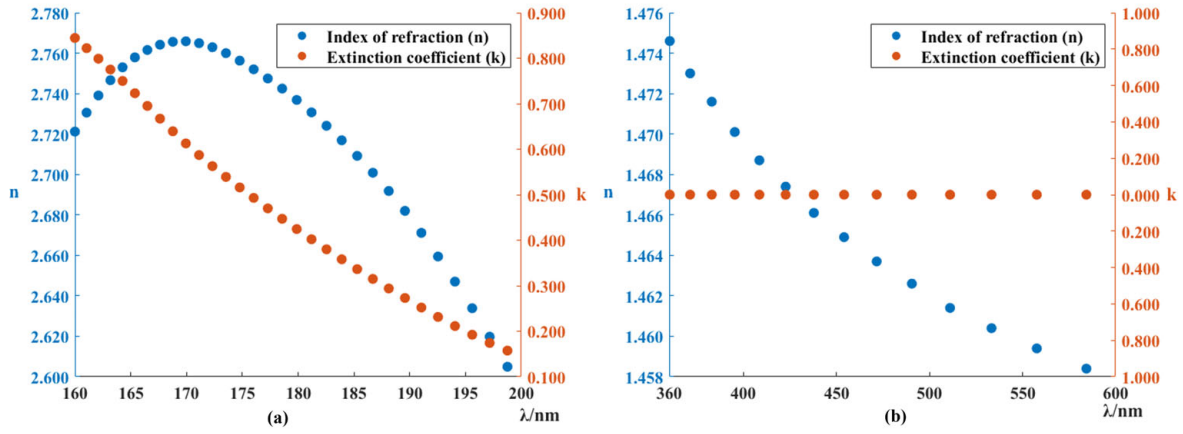

Figure 2. The index of refractive (n) and extinction coefficient (k) versus wavelength of (**a**) Si_3N_4 and (**b**) SiO_2. Note that the data are from GSolver V5.2 [28].

It was assumed that the morphology of the bottom grating was linearly tilted. The slope was set as 0.01 (or ϕ was set as 0.57°). Layer A was divided into two parts—the tiled top part (see the red triangle in Figure 3a) and the bottom rectangle. The tiled top part was layered (with the number n-2 in Figure 3a). To obtain the optimal number of layers, taking the material system of SiO_2 for example, as shown in Figure 3b, we presented the relationship between the normalized ratio and the number of layers (i.e., n-2) in various diffraction orders (0th through ±4th diffraction order). Note that the layer number was counted considering Layer B (i.e., layer 1) and the bottom rectangle part of Layer A (i.e., layer 2). It can be seen that after 80 layers, the normalized ratio becomes convergent and n = 82 is employed here. Another key parameter in GSolver is the spatial harmonics, which have a significant impact on computational accuracy. Thus, we presented the relationship between the normalized ratio and the number of harmonics in various diffraction orders (0th through ±4th diffraction order). As shown in Figure 3c, the normalized ratio becomes convergent after 60, and thus, 80 is selected here.

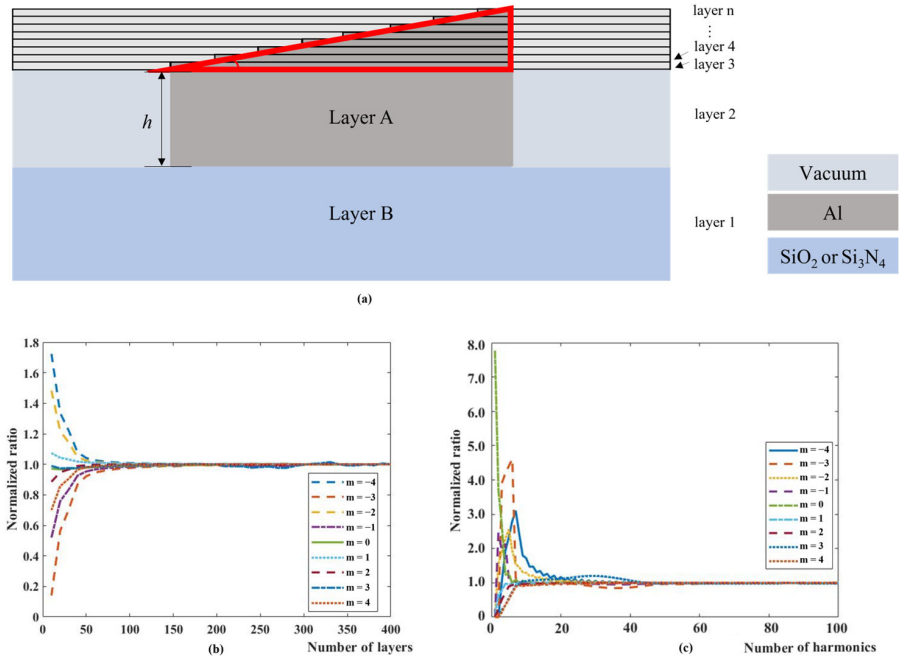

Figure 3. The creation of the model. (**a**) Geometrical shape of a layered overlay target; the relationship between the normalized ratio and the (**b**) number of layers or (**c**) the number of harmonics for various diffraction orders (the material system of SiO_2).

3. Results and Discussion

We investigated the diffraction efficiency for the symmetric and asymmetric gratings in different diffraction orders at various pitches. In addition, two overlay target material systems were explored.

3.1. Material System 1 (Layer A: Al, and Layer B: Si_3N_4)

Firstly, we conducted an analysis at the pitch of 3000 nm. As shown in Figure 4, for the symmetric grating, the diffraction efficiency difference between positive and negative diffraction orders is zero for every diffraction order. The diffraction efficiency of the ±1st diffraction order is larger than the other diffraction order; the ±3rd diffraction order is larger than that of the ±2nd and the ±4th diffraction order. When the grating undergoes asymmetric deformation, the diffraction efficiency of the positive diffraction order and negative diffraction order is no longer equal: the negative one is larger than the positive one in this case. For the ±1st diffraction order, the diffraction efficiency increased with the increase of the wavelength. For example, diffraction efficiency increased from 0.064 at a

160 nm wavelength to 0.17 at a 200 nm wavelength for the −1st diffraction order (shown by the red dashed line in Figure 4a). But for the −2nd diffraction order, the diffraction efficiency decreased from 0.014 at a 160 nm wavelength to 0.011 at a 200 nm wavelength. For the ±3rd diffraction order, a similar rising trend according to wavelength was found as the ±1st diffraction order. For the −4th diffraction order, the variations of diffraction efficiency along the wavelength were gentler than the odd diffraction orders. It is 3.9×10^{-3} at a 160 nm wavelength and 3.5×10^{-3} at a 200 nm wavelength. The asymmetric deformation has a significant impact on the diffraction efficiency for the ±1st diffraction order than the higher diffraction order ones. The maximum error signal (defined as the difference in the diffraction efficiency of positive and negative diffracted light) for higher diffraction orders can reach two orders of magnitude smaller than the ±1st diffraction order one.

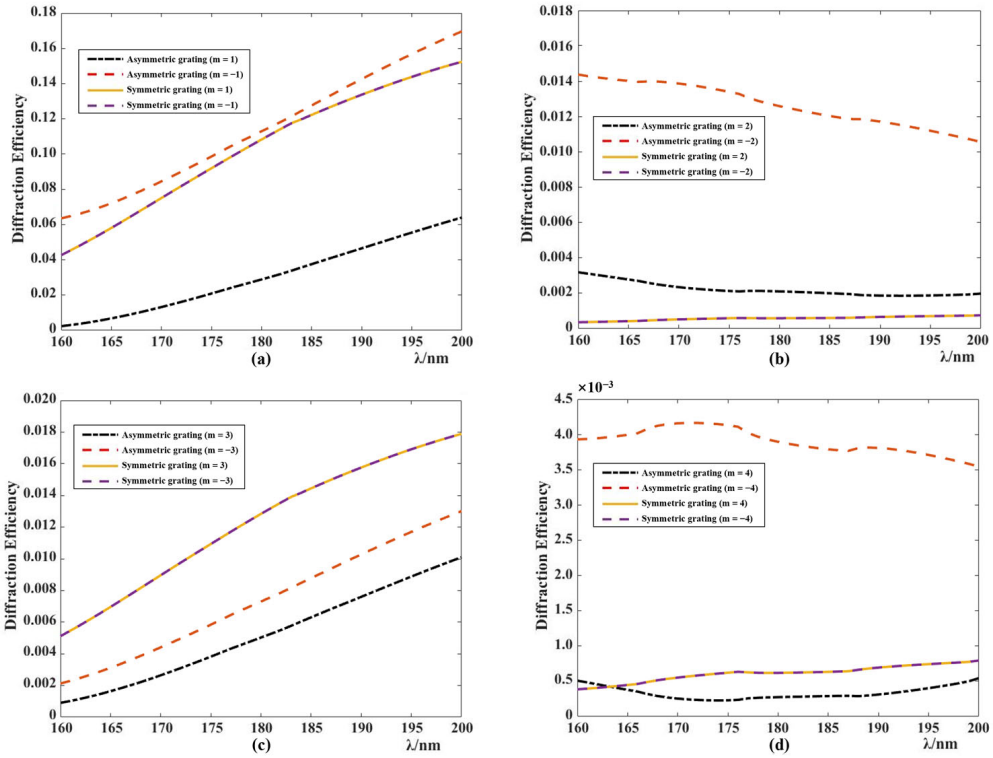

Figure 4. Simulation of diffraction efficiency for symmetric and asymmetric gratings as a function of the wavelength in different diffraction orders, m = (**a**) ±1, (**b**) ±2, (**c**) ±3, and (**d**) ±4. Pitch = 3000 nm.

To go a step further, we introduced an evaluation function (*EF*). It was defined as the ratio between the difference and sum of diffraction efficiency in a fixed diffraction order (i.e., m = 1, 2, 3, and 4) as follows:

$$EF = \left| \frac{DE_{+m} - DE_{-m}}{DE_{+m} + DE_{-m}} \right|$$

where DE_{+m} is the diffraction efficiency of $+m$ diffraction order (i.e., positive diffraction order), DE_{-m} is the diffraction efficiency of $-m$ diffraction order (i.e., negative diffraction order), and m is the diffraction order (i.e., 1 through 4).

Figure 5 presents the evaluation function for an asymmetric grating at various wavelengths for different diffraction orders. For the odd diffraction order, the evaluation function decreased with the increase of the wavelength. For the ±2nd diffraction order, the evaluation function is not sensitive to the wavelength. The value of the evaluation function for the ±2nd diffraction order or the ±3rd diffraction order is smaller than that for the ±1st diffraction order throughout the whole wavelength range (i.e., 160–200 nm). In detail, at a 160 nm wavelength, the evaluation function is 0.93, 0.023, and 0.40 for the ±1st, the ±2nd, and the

±3rd diffraction order, respectively. But at a 200 nm wavelength, the evaluation function is 0.45, 0.034, and 0.13 for the ±1st, the ±2nd, and the ±3rd diffraction order, respectively. As for the ±4th diffraction order, in the wavelength range from 160 to 165 nm, the evaluation function value is smaller than that of the ±1st diffraction order. But from the 166 to 200 nm wavelength, the evaluation function value of the ±1st diffraction order is smaller than that of the ±4th diffraction order. The reason may be that, for the high diffraction angle at the ±4th diffraction order, it cannot meet the requirements of paraxial approximation of the model. The evaluation function of the ±1st diffraction order is ~40 times larger than the ±2nd diffraction order at a 160 nm wavelength, indicating an effective method to weaken the impact of asymmetric deformation by collecting certain high-diffraction-order light (i.e., the ±2nd diffraction order in this case).

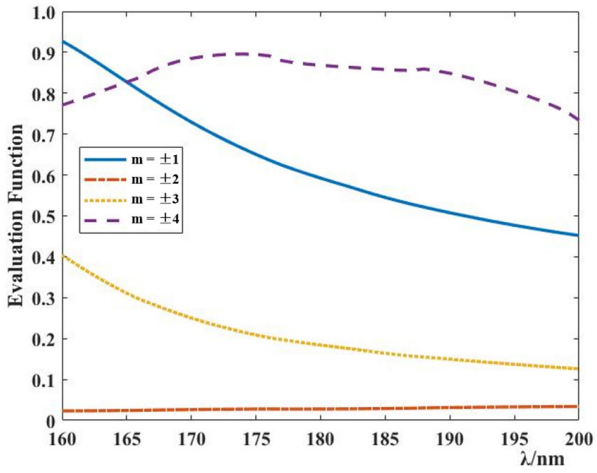

Figure 5. The wavelength dependencies of the evaluation function for an asymmetric grating in different diffraction orders. Pitch = 3000 nm.

Subsequently, we decreased the pitch to 1600 nm. As shown in Figure 6, a similar result was obtained for the symmetric grating as in the case of the pitch of 3000 nm. For the grating with an asymmetric deformation, the diffraction efficiency of the positive one (illustrated by a black dashed line in Figure 6) is smaller than the negative one (illustrated by a red dashed line in Figure 6). The diffraction efficiency of the odd diffraction order is on the increase with an increasing wavelength. For example, for the −1st diffraction order, at a 160 nm wavelength, the diffraction efficiency is 0.049; at a 200 nm wavelength, it increases to 0.17 (illustrated by a red dashed line in Figure 6a). The diffraction efficiency of the negative even diffraction order has a trend to increase first and then decrease with the increase of the wavelength. The value of the evaluation function for the ±3rd diffraction order (shown by the yellow dotted line in Figure 7) is the smallest with a wavelength range of 160 to 200 nm for a pitch of 1600 nm.

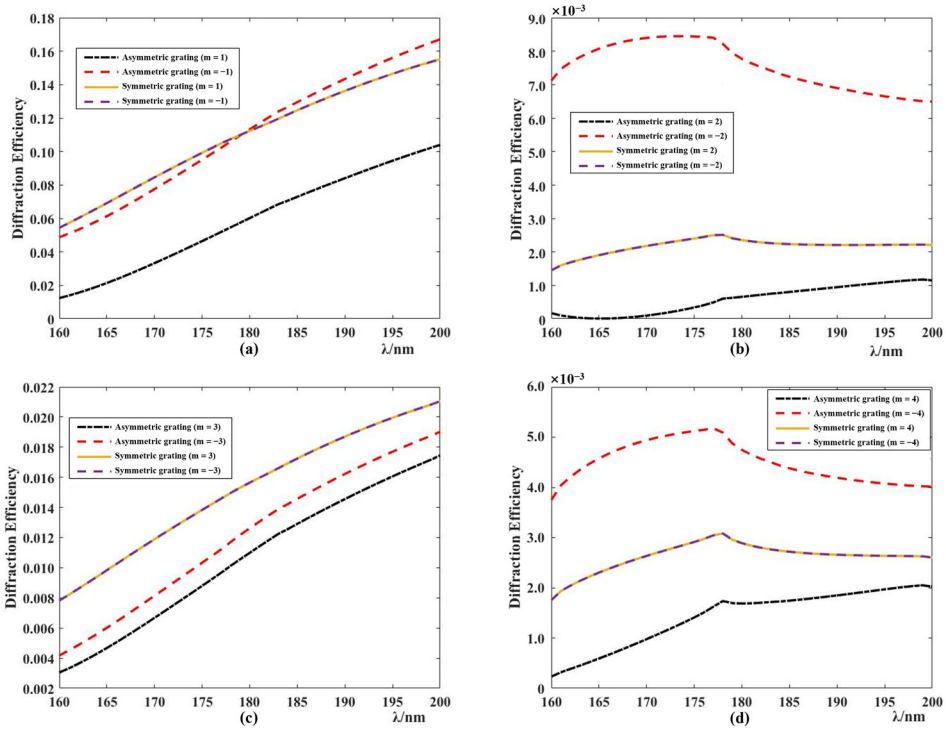

Figure 6. Simulation of diffraction efficiency for symmetric and asymmetric gratings as a function of the wavelength in different diffraction orders; m = (**a**) ±1, (**b**) ±2, (**c**) ±3, and (**d**) ±4. Pitch = 1600 nm.

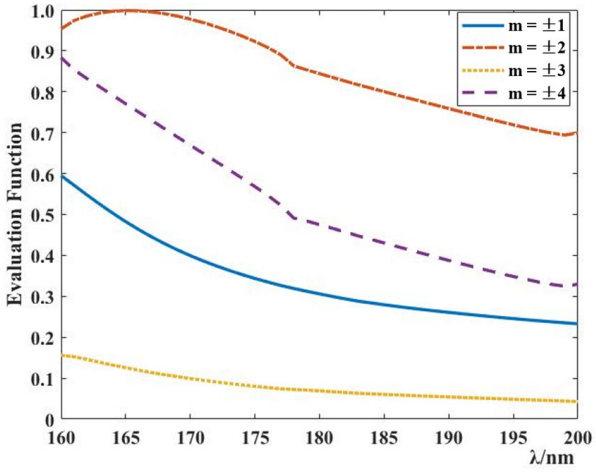

Figure 7. Evaluation function for an asymmetric grating at various wavelengths for different diffraction orders. Pitch = 1600 nm.

Likewise, a pitch of 1000 nm was used. A similar result was obtained for the symmetric grating, where the diffraction efficiency of positive diffraction order is equal to the negative one (see the yellow solid line and purple dashed line in Figure 8). For the asymmetric grating, the diffraction efficiency of the negative diffraction order is larger than the positive one. An upward trend of the diffraction efficiency with the increase of the wavelength was observed for all diffraction orders at the pitch of 1000 nm. From Figure 9, we can see that the ±3rd diffraction order shows the smallest value of evaluation function than the other diffraction orders, except for the ±4th diffraction order at an approximate 196 nm wavelength.

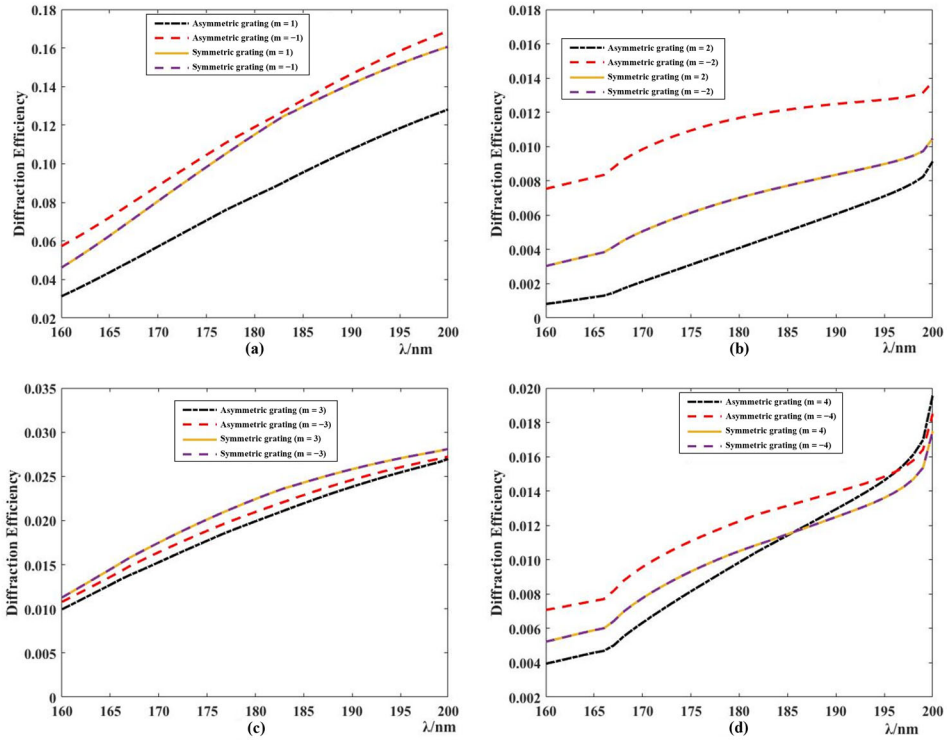

Figure 8. Simulation of diffraction efficiency for symmetric and asymmetric gratings with respect to the wavelength in different diffraction orders; m = (**a**) ±1, (**b**) ±2, (**c**) ±3, and (**d**) ±4. Pitch = 1000 nm.

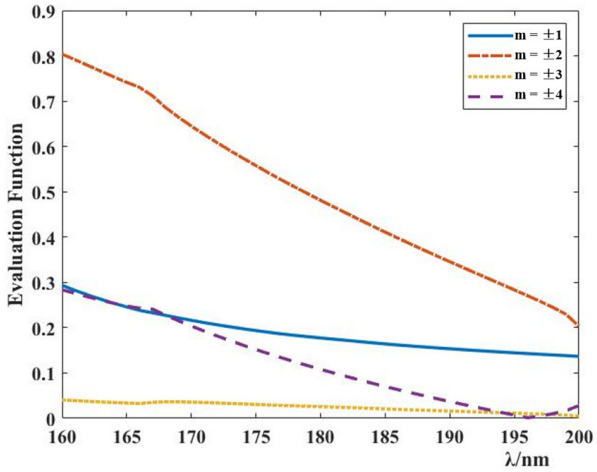

Figure 9. Dependence of the evaluation function for an asymmetric grating on the wavelength in different diffraction orders. Pitch = 1000 nm.

However, with a decrease of pitch (i.e., 600 nm), we cannot obtain the diffraction efficiency value from the model of the ±4th diffraction order, but rather the ±1st, the ±2nd, and the ±3rd diffraction orders. For the ±1st and the ±2nd diffraction orders, the diffraction efficiency takes on an upward tendency with the increase of the wavelength (see Figure 10a,b). But for the ±3rd diffraction order, it displays the tendency to rise up at the beginning and then decline when increasing the wavelength (Figure 10c). As can be seen in Figure 10d, the ±3rd diffraction order exhibits the minimum value of the evaluation function.

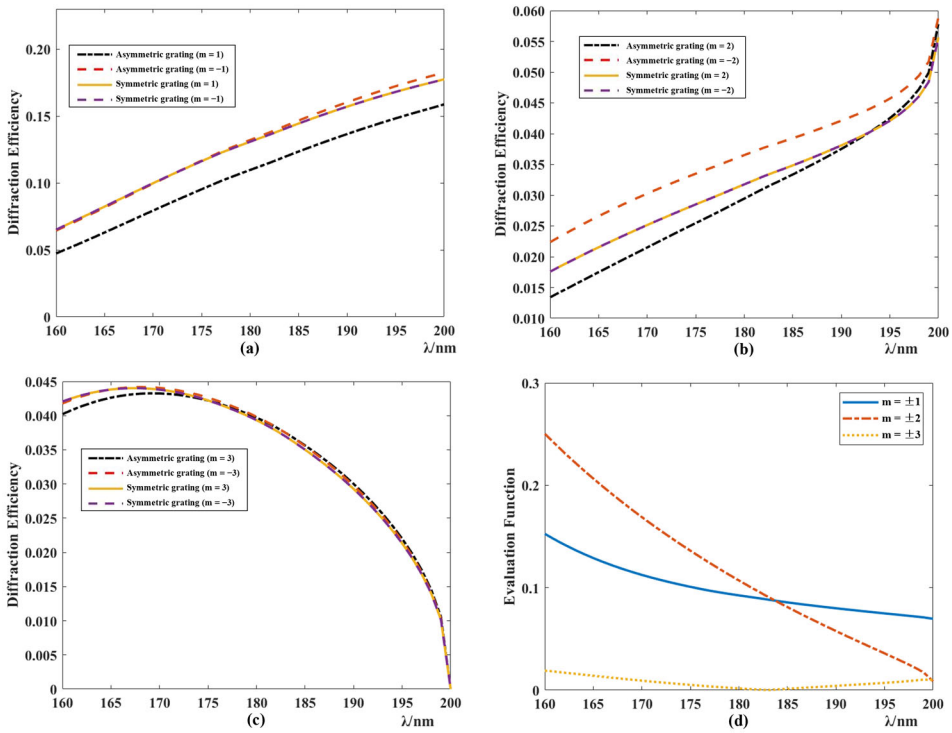

Figure 10. Simulation of diffraction efficiency for symmetric and asymmetric gratings in dependency of the wavelength in different diffraction orders; m = (**a**) ±1, (**b**) ±2, (**c**) ±3. (**d**) Evaluation function for an asymmetric grating at various wavelengths and diffraction orders. Pitch = 600 nm.

At a given pitch, the optimal diffraction order can be selected to have the minimum value of the evaluation function, thus mitigating the impact of asymmetric deformation on overlay metrology. When the value of pitch is smaller than 1600 nm, the ±3rd diffraction order is the optimal choice, but for a large value of a pitch (i.e., 3000 nm), the ±2nd diffraction order can be considered.

3.2. Material System 2 (Layer A: Al, and Layer B: SiO_2)

To expand the material-selecting scope for the overlay target, we carried out an analysis of a second material system with Layer A of Al and Layer B of SiO_2. To go one step further, we continued to increase the pitch to 6000 nm in a broad wavelength range from 360 to 600 nm.

As displayed in Figure 11, for all diffraction orders (i.e., ±1st through ±4th), the diffraction efficiency difference between positive and negative diffraction orders of the symmetric grating is zero (see the yellow solid line and purple dashed line in Figure 11). The diffraction efficiency of the ±1st diffraction order is the largest. But for the asymmetric grating, the diffraction efficiency of the positive and negative diffraction orders is no longer equal, where the negative one (see the red dashed line in Figure 11) is larger than the positive one (see the black dashed line in Figure 11), except for the ±4th diffraction order. The diffraction efficiency shows a trend of decreasing with increased wavelength, except for the +1st and the +3rd diffraction orders (see the black dashed line in Figure 11a,c). For instance, at a 360 nm wavelength, the diffraction efficiency is 0.21, and at a 600 nm wavelength, it decreased to 0.14 for the −1st diffraction order. For the −2nd diffraction order, it is 8.5×10^{-3} at a 360 nm wavelength and 2.4×10^{-3} at a 600 nm wavelength. The asymmetric deformation has a greater impact on the diffraction efficiency for the ±1st diffraction order than for the other diffraction orders, just as in the case of material system 1.

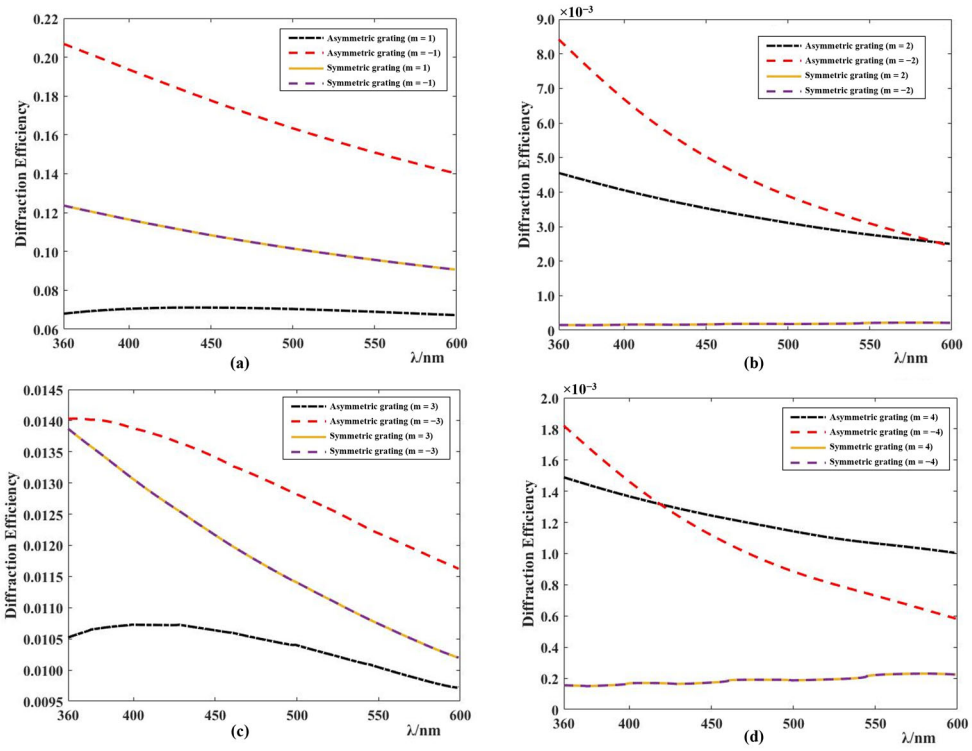

Figure 11. Simulation of diffraction efficiency for symmetric and asymmetric gratings vs. wavelength in different diffraction orders; m = (**a**) ±1, (**b**) ±2, (**c**) ±3, and (**d**) ±4. Pitch = 6000 nm.

Figure 12 displays the evaluation function at various wavelengths and diffraction orders for an asymmetric grating at the pitch of 6000 nm. From 360 to 486 nm, the ±4th diffraction order has the minimum evaluation function; from 487 to 507 nm, the ±3rd diffraction order exhibits the minimum evaluation function; and from 508 to 600 nm, the ±2nd diffraction order displays the minimum evaluation function.

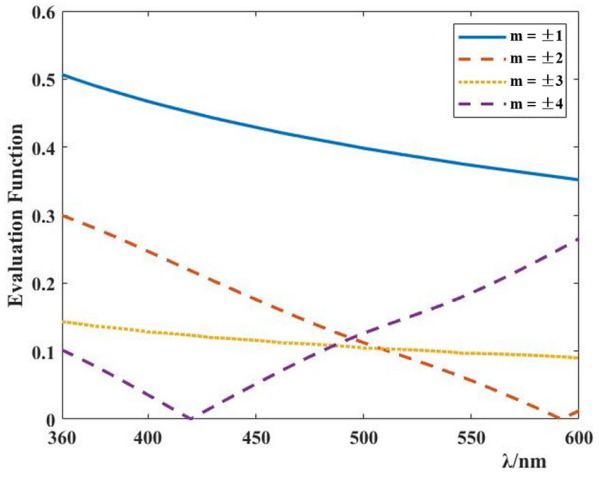

Figure 12. Evaluation function for an asymmetric grating at various wavelengths and diffraction orders. Pitch = 6000 nm.

3.3. Summary of the Material Systems

As shown in Table 1, we presented a guideline for selecting the optimal diffraction order considering the wavelength, pitch, and overlay target materials. We can see that the optimal diffraction order is pitch-dependent. When the value of the pitch is smaller than 1600 nm, for the wavelength range from 160 to 200 nm, the ±3rd diffraction order is the

optimal choice, but for a pitch of 3000 nm, the ±2nd diffraction order can be considered for the Si_3N_4 material system. For the SiO_2 material system, at a fixed pitch (e.g., 6000 nm), the optimal diffraction order depends on the wavelength.

Table 1. Summary of selecting the optimal diffraction order considering wavelength, pitch, and overlay target materials.

Wavelength/nm	Pitch/nm	The Optimal Diffraction Order
		Layer A: Al and Layer B: Si_3N_4
160–200	3000	±2nd
160–200	1600	±3rd
160–200	1200	±3rd
160–200	600–1000 (step size: 100 nm)	±3rd
		Layer A: Al, and Layer B: SiO_2
360–486	6000	±4th
487–507	6000	±3rd
508–600	6000	±2nd

4. Conclusions

In conclusion, using the RCWA method, we demonstrated that selecting certain high diffraction orders can mitigate the influence of asymmetric grating on overlay metrology. We introduced an evaluation function to explain the asymmetric signal obtained from the deformed grating. Compared with the ±1st diffraction order, the ±2nd and ±3rd diffraction orders are optimal diffraction orders, but the ±4th diffraction order is not robust. The asymmetric signal is pitch-dependent. For the wavelength range from 160 to 200 nm, when the value of the pitch is smaller than 1600 nm, the ±3rd diffraction order is the optimal choice, but at a pitch of 3000 nm, ±2nd is the optimal one for the Si_3N_4 material system. For the SiO_2 material system, at a fixed pitch (e.g., 6000 nm), the optimal diffraction order depends on the wavelength. The diffraction order with the minimum value of the evaluation function at different pitches, wavelengths, and overlay target materials is provided, which is useful for future overlay metrology development. This topic is significant in the improvement of advanced metrology for photolithography, thus decreasing the EPE and, hence, enhancing the yield of HVM.

Author Contributions: Methodology, W.Y.; Validation, W.Y. and S.Y.; Formal analysis, W.Y.; Investigation, W.Y. and S.Y; Resources, W.Y.; Data curation, W.Y.; Writing—original draft, J.C.; Writing—review & editing, J.C.; Supervision, N.L.; Project administration, N.L. All authors have read and agreed to the published version of the manuscript.

Funding: This research received no external funding.

Institutional Review Board Statement: Not applicable.

Informed Consent Statement: Not applicable.

Data Availability Statement: The data presented in this study are available upon request from the corresponding author. The data are not publicly available due to laboratory regulations.

Conflicts of Interest: The authors declare no conflicts of interest.

References

1. Wischmeier, L.; Graeupner, P.; Kuerz, P.; Kaiser, W.; van Schoot, J.; Mallmann, J.; de Pee, J.; Stoeldraijer, J. High-NA EUV lithography optics becomes reality. *Proc. SPIE* **2020**, *11323*, 1132308.
2. Ngo, A.; Dey, B.; Halder, S.; Gendt, S. Machine learning-based edge placement error analysis and optimization: A systematic review. *IEEE Trans. Semicond. Manuf.* **2023**, *36*, 1–13. [CrossRef]
3. Macka, C.A.; Adelb, M.E. Overlay and edge placement error metrology in the era of stochastics. *Proc. SPIE* **2023**, *12496*, 1249609.
4. Slotboom, D.M.; Hinnen, P.; Mulkens, J. On-product overlay solutions for DUV and EUV mix-scanner usage in an EPE-driven patterning world. *Proc. SPIE* **2022**, *12051*, 120510L.

5. Mulkens, J.; Slachter, B.; Kubis, M.; Tel, W.; Hinnen, P.; Maslow, M.; Dillen, H.; Ma, E.; Chou, K.; Liu, X.; et al. Holistic approach for overlay and edge placement error to meet the 5nm technology node requirements. *Proc. SPIE* **2018**, *10585*, 105851L.
6. Bhattacharyya, K. Tough road ahead for device overlay and edge placement error. *Proc. SPIE* **2019**, *10959*, 1095902.
7. Jee, T.; You, J.; Lee, H.; Lee, S.; Hong, S.; Seo, J.; Meir, R.; Oved, N.; Park, J.; Kim, S.; et al. Budgeting and predicting pattern defects using edge placement error and machine learning. In Proceedings of the 2023 7th IEEE Electron Devices Technology & Manufacturing Conference (EDTM), Seoul, Republic of Korea, 7–10 March 2023.
8. Shchegrov, A.; Leray, P.; Paskover, Y.; Yerushalmi, L.; Megged, E.; Grauer, Y.; Gronheid, R. On product overlay metrology challenges in advanced nodes. *Proc. SPIE* **2020**, *11325*, 113251P.
9. Jin, H.; Qi, Y. Review of overlay error and controlling methods in alignment system for advanced lithography. *Proc. SPIE* **2022**, *12478*, 1247843.
10. Zhang, J.; Chen, X.; Yang, T.; Liu, S. X-ray-based overlay metrology using reciprocal space slicing analysis. *Opt. Lett.* **2023**, *48*, 6380–6383. [CrossRef]
11. Park, D.; Kim, H.; Seo, M.; Ju, J.; Kim, Y.; Shahrjerdy, M.; Leest, A.; Soco, A.; Miceli, G.; Massier, J.; et al. Unique method for controlling device level overlay with high-NA optical overlay technique using YieldStar in a DRAM HVM environment. *Proc. SPIE* **2018**, *10585*, 105850V.
12. Koonmen, J. Applications products and business opportunity. In *ASML Small Talk*; ASML: Veldhoven, The Netherlands, 2021.
13. Su, C.; Lin, Z.; Lin, Y.; Kuo, H. Enhancement of diffraction-based overlay model for overlay target with asymmetric sidewall. *IEEE Trans. Semicond. Manuf.* **2020**, *33*, 373–382. [CrossRef]
14. Li, R.; Hsu, I.; Brożek, T.; Yang, L.; He, D.; Wu, F.; Ren, J.; Zhu, Y.; Zhang, Y.; Liu, P.; et al. In-line monitoring of overlay and process window using design-assisted voltage contrast inspection for 14 nm FINFET technology. *Proc. SPIE* **2022**, *12053*, 120531U.
15. Shchegrov, A.; Leray, P.; Passover, Y.; Yerushalmi, L.; Megged, E.; Grauer, Y.; Gronheid, R. Optical overlay metrology trends in advanced nodes. *Proc. SPIE* **2022**, *12053*, 120530N.
16. Eyring, S.; Selvanathan, D.; Blanton, W.; Shuall, N.; Laske, F. Multi-layer, any-shape on-device overlay metrology. *Proc. SPIE* **2022**, *PC12053*, PC120530P.
17. Lee, H.; Chang, H.; Shin, H.; Choi, O. Image-based overlay target design using a grating intersection. *J. Micro/Nanopatterning Mater. Metrol.* **2022**, *21*, 034801. [CrossRef]
18. Blancquaert, Y.; Dezauzier, C. Diffraction based overlay and image based overlay on production flow for advanced technology node. *Proc. SPIE* **2013**, *8681*, 86812O.
19. Dasari, P.; Li, J.; Hu, J.; Smith, N.; Kritsun, O. Diffraction-based overlay metrology for double patterning technologies. *Proc. SPIE* **2009**, *7272*, 727212.
20. Mathijssen, S.; Davis, T.; Boef, A.; Bhattacharyya, K. Fundamental understanding of the interplay between target and sensor brings diffraction based overlay to the next level of accuracy. *Proc. SPIE* **2021**, *11611*, 1161121.
21. Matsunobu, M.; Nishiyama, T.; Inoue, M.; Housley, R.; Bozdog, C.; Lim, J.; Watson, B.; Reece, J.; McCandless, S.; Zwier, O.; et al. Novel diffraction-based overlay metrology utilizing phase-based overlay for improved robustness. *Proc. SPIE* **2021**, *11611*, 1161126.
22. Hsieh, H.; Cheng, J.; Yeh, Y. Optimized wavelength selection for diffraction-based overlay measurement by minimum asymmetry factor variation with finite-difference time-domain simulation. *Appl. Opt.* **2022**, *61*, 1389–1397. [CrossRef]
23. Bian, Y.; Guan, X.; Liu, B.; Guo, X.; Zhang, C.; Zhou, W.; Huang, J.; Zhang, Y.; Guo, L.; Liu, F.; et al. A study of overlay accuracy improvement on process induced asymmetry effect. In Proceedings of the 2021 International Workshop on Advanced Patterning Solutions (IWAPS), Foshan, China, 12–13 December 2021.
24. Li, Y.; Wei, Y.; Wu, Q.; Liu, X.; Wang, Q. A study of diffraction-based overlay (DBO) on a 3 nm CFET metal layer. *Proc. SPIE* **2023**, *12496*, 124962Y.
25. Xu, B.; Wu, Q.; Chen, R.; Dong, L.; Zhang, L.; Wei, Y. A study on diffraction-based overlay measurement based on FDTD method. *Proc. SPIE* **2021**, *11611*, 116113B.
26. Hinnen, P. *YieldStar Metrology System Applications for Advanced Process Control*; ASML: Veldhoven, The Netherlands; IMEC: Leuven, Belgium, 2018.
27. Mohamad, H.; Essaidi, S.; Blaize, S.; Macias, D.; Benech, P.; Morand, A. Fast Fourier factorization for differential method and RCWA: A powerful tool for the modeling of non-lamellar metallic diffraction gratings. *Opt. Quant. Electron.* **2020**, *52*, 127. [CrossRef]
28. GSolver. Diffraction Grating Analysis for Windows. Available online: https://gsolver.com/ (accessed on 8 March 2024).